FROM THE DEPARTMENT OF RADIATION PHYSICS, KAROLINSKA INSTITUTET, S-104 01 STOCKHOLM, AND THE DEPARTMENT OF RADIATION PHYSICS, UNIVERSITY OF UMEÅ, S-901 85 UMEÅ, SWEDEN.

RADIATION BEAM CHARACTERISTICS OF A 22 MeV MICROTRON

A. BRAHME and H. SVENSSON

The performance of the first 22 MeV medical microtron, the installation, and some beam data were reported by SVENSSON et coll. (1977). It was pointed out that the unique combination of a high dose rate, as in the linear accelerator, and a low energy spread of the electrons, as in the betatron, makes the microtron an attractive radiation source for a medical accelerator. In this report a more general and detailed analysis of the electron and photon dose distributions in the 22 MeV microtron is presented. Comparisons with absorbed dose distributions from other types of accelerators are also made, and the main components of the accelerator and the treatment facility which are of importance for the quality of the dose distributions are described.

Microtron and treatment facility

The accelerator is an S-band microtron (WERNHOLM 1964), and its method of extraction and some other characteristic features are given in Fig. 1. The electrons are extracted from orbit 10 to 42, which corresponds to energies between 5.3 and 22.5 MeV as the energy gain per turn is about 0.535 MeV. In principle the electrons could be extracted in any of these orbits, but the choice has for practical reasons been restricted to 9 energies at steps of about 2 MeV. Only two of these energies can be used in the photon mode of irradiation (any two of 6, 10 or 21 MeV). This relatively high number of fixed energies allows efficient use of the sharp fall-off in

Submitted for publication 7 June 1978.

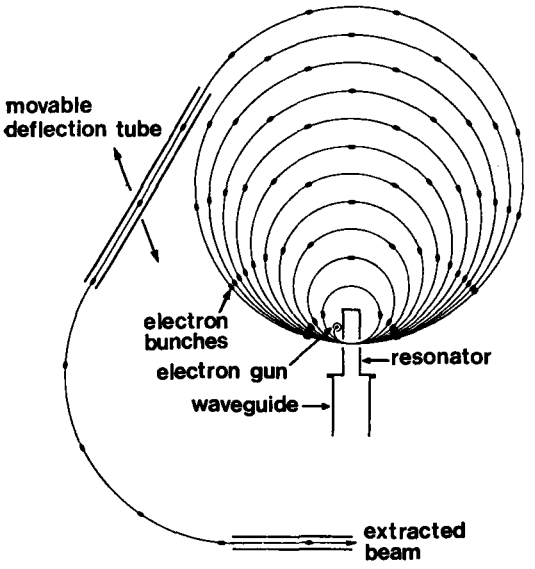

Fig. 1. The 22 MeV microtron has 42 electron orbits of which 11 appear in the figure. Diameter of the magnet 2.2 m. Extraction is made through a deflection tube which could be moved to any of the orbits between 10 and 42. The electrons leave the magnetic field at a common position independent of the position of the deflection tube. The extracted beam can either be taken into a gantry for radiation treatment or to a research facility (Brahme & Svensson 1976 a).

dose beyond the therapeutic range in the electron beams from the microtron (SVENSSON et coll. 1977).

The accelerator principle implies a stable and well-defined electron energy independent of accelerator beam current with a very low energy spread of 35 keV (FWHM) and practically no electrons outside ± 45 keV. The low energy spread facilitates the beam transport to and in the gantry. Furthermore, the beam can be transported over long distances from one microtron to different treatment rooms (Baroncelli 1974). The 22 MeV microtron which has been used in most of the present measurements makes use of the beam in one gantry for radiation therapy and in a research facility for isotope production and beam developments. A further advantage with the low energy spread is observed in the electron dose-distributions which are improved somewhat compared to those from accelerators with a broader spectral distribution (BRAHME et coll. 1975, BRAHME & SVENSSON 1976 a).

Electron beam

The distribution of absorbed dose in an electron beam should ideally be as uniform as possible over the whole target volume and outside this as rapidly as possible decrease to zero. This philosophy was followed when different parameters were defined from the absorbed dose distributions in order to give figures of merit for various electron dose distributions (BRAHME & SVENSSON 1976 a).

Definitions. Different parameters are defined in Fig. 2 on a typical central axis depth dose curve for a broad 10 MeV electron beam. Of special interest are the

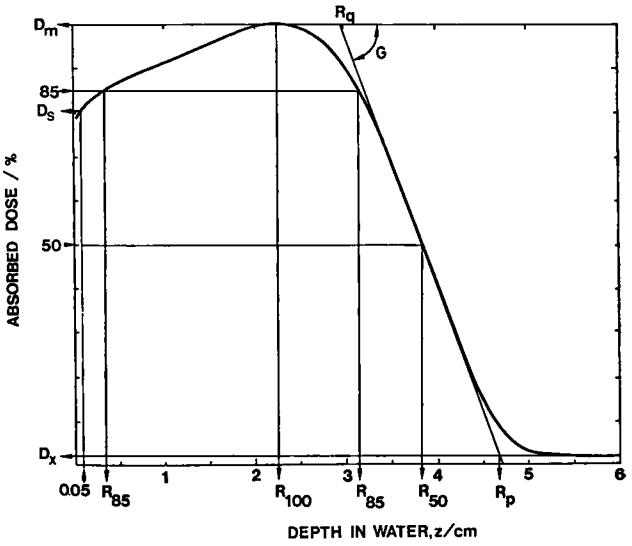

Fig. 2. Therapeutic depth-absorbed-dose distribution with definitions of all parameters used in the text. D_m = level of maximum absorbed dose. D_s = surface dose measured at 0.05 cm depth. D_x = photon background. G = dose gradient. (cf. eq. 1). R_{100} = depth of dose maximum. R_{85} = therapeutic range. R_{50} = half-value depth. R_p = practical range. R_q = extrapolation depth (cf. Table 2 ***).

therapeutic range, R_{85}, defined by the depth interval where the absorbed dose exceeds 85 per cent of its maximum value, and the dose gradient G, which is a normalized measure of the slope of the fall-off section of the depth dose curve. In the plane perpendicular to the beam the distribution of absorbed dose is conveniently described by the uniformity index. This parameter has recently been redefined as the ratio of the areas inside the 90 and 50 per cent isodose levels measured at the reference depth, taking the dose on the central axis as 100 per cent (NACP 1977).

General description of degraded electron beams. The distribution of absorbed dose along the central axis of an electron beam is greatly influenced by the presence of degrading materials in and along the beam such as scattering foils, transmission monitors, collimators and air (KARZMARK et coll. 1960, SVENSSON 1971, BRAHME 1971, BRIOT & DUTREIX 1976). These materials influence the electron fluence in three different ways, namely: by lowering and widening of the electron energy distribution, by generation of collimator scattered electrons making large angles with the central axis of the beam and, finally, by production of contaminating photons.

When the beam geometry is carefully designed, the energy degradation of the beam, characterized for example by the energy spread, generally has the dominating influence on the absorbed dose distribution. The oblique collimator scattered electrons depend to a great extent on beam geometrical factors such as effective source size, collimating materials and collimation geometry, and may be described by the mean square scattering angle of the beam reaching the phantom or the patient. When the number of degraded and obliquely incident electrons is large,

the depth of dose maximum is displaced towards the surface and the dose gradient is decreased considerably. These two phenomena are treated in more detail in the following.

The contaminating bremsstrahlung photons, finally, are mainly generated in scattering foils and other materials in the beam. The fraction of the dose due to contaminating photons depends on the scattering material used and increases almost linearly with its thickness as a result of increased bremsstrahlung production and simultaneous loss of electrons. In the following analysis the effect of the contaminating photons is taken into account by subtraction of the photon background in the definition of the dose gradient.

The normalized dose gradient G is obtained by multiplying the maximum dose gradient of the fall-off of the dose distribution by the practical range divided by the difference in absorbed dose between dose maximum and photon background (BRAHME & SVENSSON 1976 a), (cf. Fig. 2):

$$G = \left|\frac{dD}{dz}\right|_{max} \frac{R_p}{D_m - D_x} \tag{1}$$

For wide monoenergetic electron beams this normalized dose gradient has a very small energy dependence as the decrease in absolute dose gradient with increasing energy is almost compensated for by the multiplication with the practical range (BRAHME & SVENSSON 1976 a). The normalized dose gradient is therefore a useful figure of merit when comparing the fall-off sections of dose distributions from different accelerators. However, the dose gradient concept is of much more general applicability particularly when used on broad beams (with a diameter $\geqslant 10$ cm at 10 MeV and $\geqslant 15$ cm at 40 MeV) where the shape of the fall-off section no longer varies with field size (MARKUS 1964, NACP 1972).

Dose gradient of degraded beams. For broad monoenergetic and parallel electron beams the normalized dose gradient varies slowly in the range 3.0 to 3.5 for energies between 5 and 40 MeV and SSD of 100 cm (BRAHME & SVENSSON 1976 a). The dose gradient G of a degraded electron beam of most probable energy E_p and practical range R_p, obtained by degrading an initially monoenergetic and parallel beam of energy E_0 by a layer ΔR of phantom material, may be related to the dose gradient G_0 of the monoenergetic beam as was shown by BRAHME & SVENSSON (1976 a):

$$G = \frac{R_p}{R_p + \Delta R} G_0 = \frac{G_0}{1 + \frac{\Delta R}{R_p}} \tag{2}$$

The reduction of the dose gradient in the degraded beam is caused by two different processes in the layer ΔR. The first is due to the widening of the energy distribution by energy loss straggling and the second is due to widening of the angular

distribution by multiple scattering interactions. The increased width of the energy distribution can be characterized by the full width at half maximum of the energy distribution

$$\Gamma = (E_0 - E_p)/c \tag{3}$$

The constant c, which relates the energy spread to the most probable energy loss obtained in the phantom material, has a value of approximately 5 for water according to the theories of LANDAU (1944), BLUNCK & WESTPHAL (1951) and Monte Carlo calculations by BERGER (1969).

The angular distribution is best characterized by the mean square scattering angle $\bar{\theta}^2 = T\Delta R$, where T is the linear scattering power of the medium (BRAHME 1972, ICRU 1972). If it is assumed that a fraction ε of the decrease in dose gradient is caused by the energy spread and consequently a fraction $(1-\varepsilon)$ caused by the angular spread eq. (2) may be rewritten:

$$G = \frac{G_0}{1 + \varepsilon \frac{c\Gamma}{E_p} + (1-\varepsilon)\frac{\bar{\theta}^2}{TR_p}} \tag{4}$$

when a linear energy range relation is assumed. In clean therapeutic electron beams the angular spread of the electrons at the surface $\bar{\theta}^2$ is very small as the degrading scattering foils are placed at long distances from the surface and thus act as a small source of nearly parallel electrons.

For therapeutic electron beams the energy spread is generally made up of several contributions.

$$\Gamma = \Gamma_{acc} + \Gamma_{foil} + \Gamma_{air} \tag{5}$$

where Γ_{acc} originates from the crude accelerator beam, Γ_{foil} from vacuum window, scattering foils, transmission monitors etc. and Γ_{air} finally from the air. The energy spread produced in the scattering foils and other components can also be calculated from the theory mentioned (BLUNCK & WESTPHAL 1951), and a relation similar to eq. (3) may be obtained. However, the constant c will have a substantially smaller value for high atomic number materials than for the low atomic number phantom materials, being typically as low as 2 to 3 for materials like uranium, lead and gold (BERGER).

For determination of the dependence of the dose gradient on energy spread, depth dose and energy distribution data are given in Fig. 3 and Table 1 for two almost monoenergetic electron beams and two beams degraded by about 2 cm of carbon. The degraded beams are both produced from almost monoenergetic electrons decelerated by the same surface density of low atomic number materials, mainly carbon. The nearly monoenergetic beam with $(E_p)_0 = 13.6$ MeV has almost the same practical range as the degraded beams. For one of the degraded beams the energy distribution data were obtained from measurements with a scintillation spectro-

Table 1

Characteristics of nearly monoenergetic and degraded electron beams

Accelerator Material in beam (g/cm²)	E_a MeV	Γ_a MeV	R_p cm	$(E_p)_o$ MeV*	R_{50} cm	E_o MeV**	R_{85} cm	R_q cm	G —***	Γ_o MeV	D_x %
Microtron, Fig. 3 curve 1 0.16 Al + 0.10 Au + 0.12 air	20.9	0.04	10.1	20.1	8.6	20.0	7.3	7.1	3.4	0.2	2.7
Microtron, Fig. 3 curve 2 0.05 Al + 0.10 Au + 0.12 air	14.4	0.04	6.7	13.6	5.7	13.3	4.8	4.6	3.3	0.2	1.7
Microtron, Fig. 3 curve 3 0.05 Al + 3.42 C + 0.12 air	19.8	0.04	6.6	13.4	5.3	12.3	4.4	4.1	2.7	1.6	3.1
Betatron**** 3.60 C	19.9	0.01		13.7		12.2				1.6	

* Derived from MARKUS (1964), $R_p = k(E_p)_o - 1$; $k = 0.521$ cm MeV^{-1}; $1 = 0.376$ cm;
** Derived from BRAHME & SVENSSON (1976 a), $R_{50} = cE_o$; $c = 0.43$ cm MeV^{-1};
*** Derived from BRAHME & SVENSSON (1976 a), $G = (R_p/R_p - R_q)$;
**** Measured with scintillation spectrometer (HARDER 1966).

meter (HARDER 1966). For the other beams the energy data were determined from the depth dose curve (Table 1). It is observed that good agreement is obtained between the energy parameters determined from depth dose data (R_p, R_{50}) and by the scintillation method. From the experimental energy spread of HARDER and theoretical angular spread of BRAHME (1975), the value of the dimensionless parameter ε in eq. (4) has been determined to 0.45.

Therapeutic range of degraded beams. One of the greatest disadvantages of a degraded electron beam is the decreased depth of the 90 and 80 per cent dose levels as compared to a monoenergetic beam with the same practical range. This effect can be esstimated by analyzing the therapeutic range defined here as the depth of the 85 per cent dose level. From the desirability of dose uniformity in the target volume the therapeutic range should be defined by the depth of the 90 per cent dose level (ICRU 1977) as that would give the same dose variation in depth as is often accepted across the radiation field (± 5 %). This would however necessitate the use of undesirably high electron energies, particularly for deep-seated tumours, with resulting large doses beyond the therapeutic range. A therapeutic range instead defined by the depth of the 80 per cent dose level (DIN 1975) would introduce an unacceptably

large dose variation across the target volume. For practical purposes it is therefore suggested that the depth of the 85 per cent dose level is a good compromise between these two conflicting goals of low integral dose and high uniformity.

A simple analytical expression relating the therapeutic range to the practical range can be derived when the normalized dose gradient is known and the 85 per cent dose level is assumed to be on the linear part of the depth dose curve, (cf. Fig. 2):

$$R_{85} = R_p\left(1 - \frac{0.85D_m - D_x}{G(D_m - D_x)}\right) \tag{6}$$

When the photon background D_x is less than 10 per cent of maximum absorbed dose D_m, this expression may be simplified further with less than one per cent error:

$$R_{85} = R_p\left(1 - \frac{0.85}{G}\right) \tag{7}$$

This general expression clearly shows the influence of the dose gradient, and consequently of the energy spread, on the therapeutic range. For an electron beam with a dose gradient of 3.4, which holds approximately for monoenergetic electrons between 10 and 35 MeV, the therapeutic range becomes 0.75 of the practical range.

If the expression for the dose gradient of a degraded beam, eq. (4), is inserted in eq. (7), the following relation for the therapeutic range of a beam of energy spread Γ and mean square scattering angle $\overline{\theta^2}$ is obtained:

$$R_{85}(E_p, \Gamma, \overline{\theta^2}) = R_p\left(1 - \frac{0.85}{G_0}\left(1 + \frac{\varepsilon c\Gamma}{E_p} + (1-\varepsilon)\frac{\overline{\theta^2}}{TR_p}\right)\right) \tag{8}$$

which may be rewritten:

$$R_{85}(E_p, \Gamma, \overline{\theta^2}) = R_{85}(E_p, 0, 0) - k_1\Gamma - k_2\frac{\overline{\theta^2}}{T} \tag{9}$$

where

$$k_1 = \frac{0.85R_p c\varepsilon}{G_0 E_p} \approx 0.30 \text{ cm MeV}^{-1} \tag{10}$$

and

$$k_2 = \frac{0.85(1-\varepsilon)}{G_0} \approx 0.14$$

taking

$$\frac{R_p}{E_p} = k = 0.52 \text{ cm MeV}^{-1},\ c = 5,\ \varepsilon = 0.45 \quad \text{and } G_0 = 3.4$$

For each MeV (FWHM) of energy spread in a beam, the therapeutic range is thus decreased by approximately 0.3 cm compared to a monoenergetic beam with

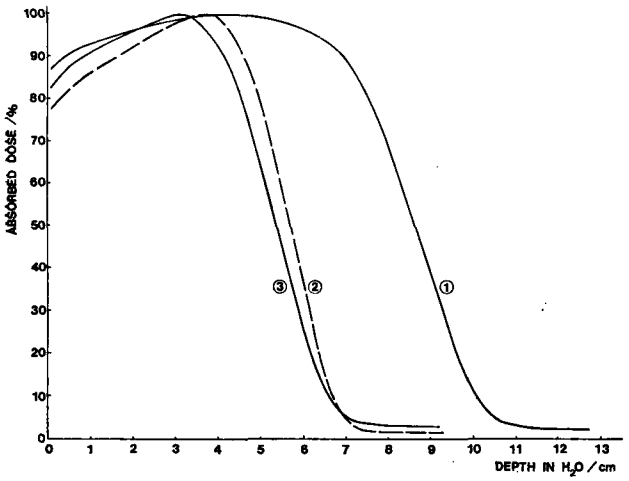

Fig. 3. Depth dose curves for degraded and nearly mono-energetic beams. In Table 1 the main parameters for the three beams are given. All the curves were measured at SSD = 100 cm and for large field sizes. Curves 2 and 3 are measured for beams with almost the same $(E_p)_0$ but differ in shape due to differences in energy spread.

the same most probable energy and consequently the same practical range as the degraded beam.

The decrease in therapeutic range due to energy spread in the beam is clearly demonstrated experimentally by the depth dose curves Nos 2 and 3 of Fig. 3 and the parameter listing of Table 1. The energy spread of the degraded beam is increased by approximately 1.4 MeV, which results in a decrease in therapeutic range of 0.4 cm compared to the nearly monoenergetic beam. The analysis is strictly valid only for monenergetic electrons that have straggled through a decelerator and obtained the Landau-Vavilov energy distributions. However, it is well known that the energy distributions of the electrons from most linear accelerators (DOLPHIN et coll. 1959, LANZL 1969, ATHERTON & CALAMINI 1976) are very similar in shape to those of straggled electrons (BLUNCK & WESTPHAL, DOLPHIN et coll., BREUER 1964). The energy spread (FWHM) is typically about 6 per cent of E_p for a travelling wave linac and 12 per cent for a standing wave linac (ATHERTON & CALAMINI).

It can thus be concluded that electron beams with identical practical ranges and consequently identical most probable electron energies E_p, will have different therapeutic ranges depending on the energy spread in the beams. At 10 MeV this means a loss in therapeutic range compared to a monoenergetic beam according to eq. (9) and (10) of 4, 2 and 0.1 mm, respectively, for a standing wave linac, a travelling wave linac and a microtron. At 20 MeV the corresponding figures become 7, 4 and 0.1 mm, as the energy spread of the microtron beam is about 0.04 MeV (FWHM) independent of the energy. Additional to the values mentioned are the losses in therapeutic range due to the energy spread produced in scattering foils, etc. and to the mean square scattering angle of the electrons. This mechanism for loss of therapeutic range due to energy spread in the beam has not been fully recognized by some authors (ATHERTON 1976, SCHRIBER et coll. 1976, BJÄRNGAARD

et coll. 1976) due to dosimetric uncertainties or crude theoretical models (BRAHME & SVENSSON 1978).

The loss of therapeutic range for a given practical range, or rather the increase in practical range necessary to obtain a given therapeutic range, may be regarded as clinically insignificant in some situations, but may be of importance when the tumour or target volume is situated close to radiation sensitive organs. When this is the case, small improvements in the dose distribution can be of considerable clinical value as the dose response relations observed for the tumour and for the normal tissues may be very sharp (HERRING & COMPTON 1971, SVENSSON et coll. 1975). This argument becomes of increasing importance since the improved diagnostic techniques available today allow more accurate dose planning and consequent efficient use of high quality radiation beams.

When the energy of a monoenergetic beam is changed from E_0 to E_p without introducing energy spread (e.g. by changing accelerator energy) the change in therapeutic range can be estimated in a way similar to the above:

$$R_{85}(E_p, 0) = (R_{p,0} - k(E_0 - E_p))\left(1 - \frac{0.85}{G_0}\right) = R_{85}(E_0, 0) - k_3(E_0 - E_p) \qquad (11)$$

where

$$k_3 = \left(1 - \frac{0.85}{G_0}\right) k \approx 0.39 \text{ cm MeV}^{-1} \qquad (12)$$

assuming no variation in the dosegradient for monoenergetic electrons from E_0 to E_p and the same values of the other parameters as before. In all practical situations when a beam is degraded by matter, energy loss and energy spread occur simultaneously, and eq. (9) and eq. (11) must be used together:

$$R_{85}(E_p, \Gamma) = R_{85}(E_0, 0) - k_3(E_0 - E_p) - k_1\Gamma \qquad (13)$$

Equation (13) is the general expression for the therapeutic range of a degraded beam when the most probable energy loss and the energy spread are known and it is assumed that the mean square scattering angle is negligible. It can thus be concluded that the loss in therapeutic range due to energy spread alone ($k_1\Gamma$) is approximately one third of the loss in therapeutic range due to a pure decrease in most probable energy ($2.5\ k_3\Gamma$) when using a high atomic number scattering foil (eq. (3), $c = 2.5$).

In the appendix eq. (13) is used to derive the maximum accelerator energy of interest when a single scattering foil is used to flatten an electron beam.

Beam geometry

In order to obtain dose distributions as similar as possible to those of plane parallel and monoenergetic beams, several beam geometrical considerations are of great importance: (1) The effective electron source size should be as small as

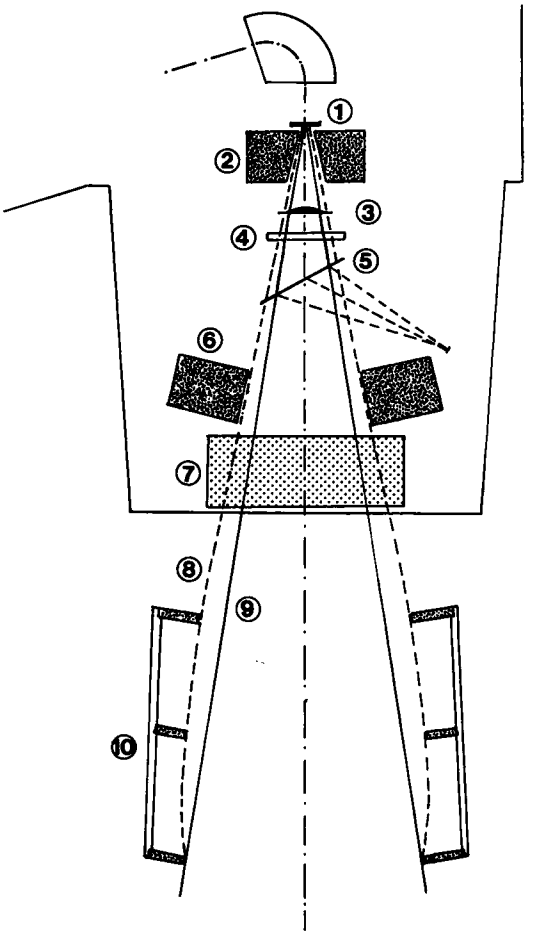

Fig. 4. The treatment head and collimating system during electron therapy. Number 1 the primary scattering foil and No. 3 the secondary scattering foil are the main scattering components in the beam flattening system. The primary collimator No. 2, the photon collimators No. 6 and No. 7 and the continuously adjustable beam shaping devices No. 10 are all placed outside the locus No. 8 of the closest allowable collimation in order not to detoriate beam uniformity. This curve (No. 8) is significantly wider than the geometrical beam No. 9. The sealed transmission chamber No. 4 and the mirror No. 5 are of very low surface density and are made of low atomic number materials in order to minimize beam degradation.

possible to simplify collimation and to avoid scattered electrons that make large angles with the beam axis, (2) the effective source to surface distance should not be decreased considerably below the standardized 100 cm, for example by scattering materials in the beam (BRAHME 1977), (3) the beam should be collimated in such a way that as few electrons as possible can be scattered into the beam from the beam limiting devices (SVENSSON, SVENSSON et coll. 1977, BRAHME 1977), and (4) The amount of degrading materials in the beam should be minimized to keep energy spread, energy loss and photon contamination low (SVENSSON, BRAHME 1972).

In order to fulfil these conditions, a dual scattering foil system (BRAHME 1972, SVENSSON & BRAHME 1976, KOZLOV & SHISHOV 1976, BRAHME 1977) is used in the microtron (Fig. 4). The primary scattering foil spreads the beam, and the secondary foil is shaped to flatten the dose distribution to a high degree of uniformity. The thickness and the shape of the foils are optimized such that the smallest possible

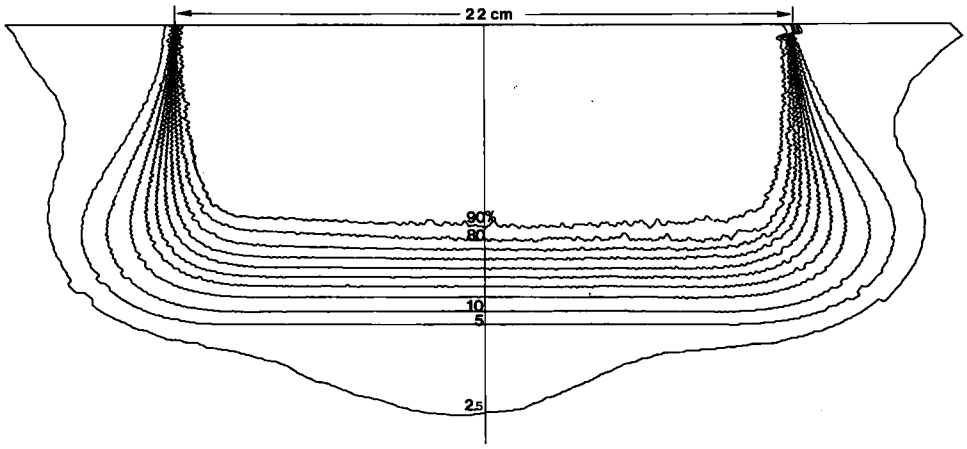

Fig. 5. Typical isodose distribution ($(E_p)_o = 21.1$ MeV, SSD = 100 cm, 22 cm × 22 cm). Measurements made with a diode in a water phantom. Original curves from the isodose-plotting system are used. The bump in the 2.5 % isodose level in the centre of the field is partly due to photons from the scattering foil. The 2.5 % level outside the field is caused by photons both from the beam limiters and the scattering foils. The photon background generated in the water phantom amounts to about 1.5 %.

amount of scattering material is placed in the beam. The secondary foil is thickest at the centre of the beam and placed fairly close to the primary foil (~10 cm) in order to make the effective source size small and the effective source to surface distance well defined and close to 100 cm.

The electron beam collimation system is designed using the air as an active component. This is so particularly at the low energies when the air effectively scatters electrons at the border of the beam back into the beam thus preserving good uniformity. The beam is simulatenously limited in size by three consecutive beam limiters which are continuously adjustable for field sizes from 36 cm × 28 cm down to 2 cm × 4 cm. All but the last beam limiters are placed outside the geometrical beam edge, where the electron fluence is relatively low. This in combination with the small effective electron source size and the small area of the beam limiters which is exposed to electrons results in a low contamination of scattered electrons in the beam (cf. Fig. 4 and BRAHME 1977). By this 'balloon' type of collimation the central axis depth dose curve is not influenced by the presence of the collimator except for the very small field sizes.

Dose distribution

Dosimetry. Depth dose distributions were measured in water phantoms with three different dosimeter systems, namely $FeSO_4$ solution in polystyrene vessels (PETTERSSON & HETTINGER 1967), a liquid ionization chamber (WICKMAN 1974) and a diode (HULTÉN 1975). No systematic difference between the measurements were obtained at depths larger than dose maximum. At small depths, i.e. from

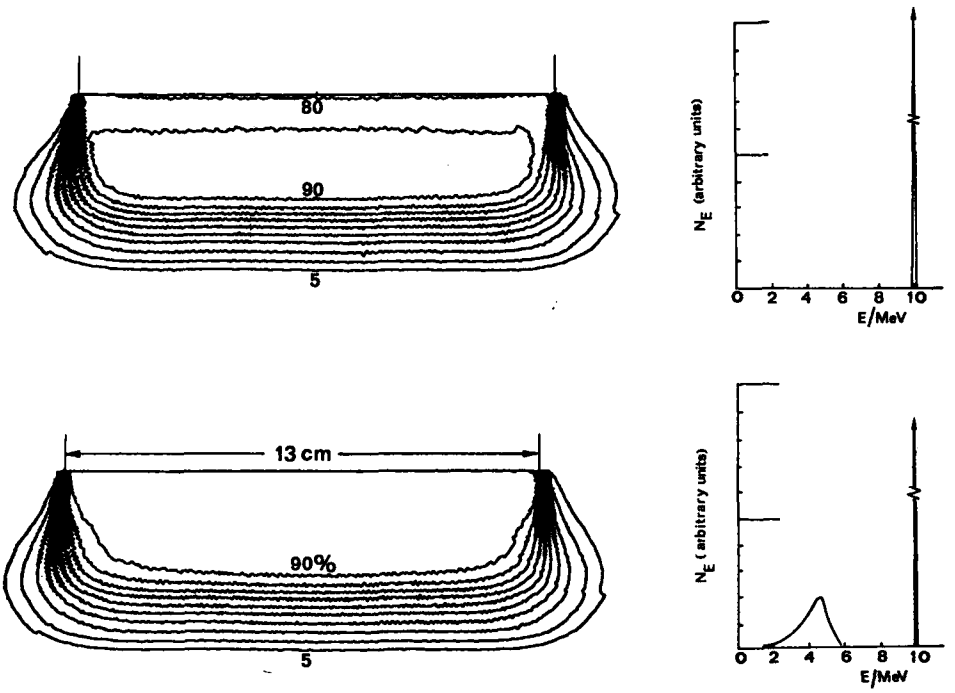

Fig. 6. Isodose distributions and accompanying electron spectra for a nearly monoenergetic beam (upper half) and a beam with a depth dose flattening filter (Brahme & Svensson 1976 c) (lower half). A considerable increase of the surface dose is noted in the lower isodose curve due to the low energy electron component in the spectrum. The spectra are representative for the situation immediately below the filter (position 3, Fig. 4).

0.05 cm to 0.5 cm, where the $FeSO_4$ dosimeter was not used, the diode measurements gave values a few per cent lower than the liquid ionization chamber (BRAHME & SVENSSON 1976 b). The distributions now reported are mostly measured with the diode technique in a water phantom. If the liquid ionization technique is regarded as the most accurate one, the reported curves may be in error by one or at the most two per cent in the near surface region due to the uncertainty of the correction applied.

Off axis flattening. It is possible with the dual foil technique to produce large uniform treatment fields with a small amount of scattering material in the beams and thus preserve a high dose gradient (Fig. 5).

An investigation of 14 betatrons in the Scandinavian countries 1968 showed that the dose homogeneities of electron beams were unacceptable for radiation treatment if the aim was to give the target a dose within some ± 5 per cent. The Nordic Association of Clinical Physics (NACP) made recommendations in order to force the manufacturers to improve dose uniformities at least on new accelerators and to

stimulate the hospital physicists to improve adjustments of scattering foils etc. The recommendations of NACP (1972) implied that the variation of the absorbed dose in a reference plane inside approximately 80 per cent of the geometrical beam area should not vary more than 15 per cent. These recommendations were a compromise as it was considered unrealistic with the accelerators available at that time to achieve a better uniformity. The uniformity index of the electron beams from the microtron varies in the interval 0.86–0.95 for the energy range 5 to 20 MeV and field sizes 10 cm × 10 cm up to 32 cm × 25 cm (Fig. 5). The present investigation thus shows that the off-axis dose variation could be kept within a few per cent over almost the complete geometrical beam with preserved high dose gradient.

Depth flattening. The relatively clean beam from the microtron (i.e., the low energy spread, the small contamination of photons, low energy electrons and electrons making large angles with the primary beam) may at low energies be inconvenient for treatment of superficial tumours, as the absorbed dose in the near surface region may be too low (Fig. 3). This is particularly so as the aim when using low energy electron radiation generally is to treat the near-skin region. Therefore, a depth dose flattening filter has been designed which increases the absorbed dose at small depths (BRAHME & SVENSSON 1976 c). The working principle of the filter is to introduce a low energy component into the electron beam by partial deceleration. The energy and the percentage low energy electrons are adjusted so that they do not influence the dose distribution at and beyond the dose maximum. The dose gradient is therefore not changed by the filter. In Fig. 6 is shown a beam with and without a depth dose flattening filter. The 90 per cent isodose is extended to the surface with the filter, and the surface dose is thus increased by more than 10 per cent.

Deceleration. For the most superficial lesions like mycosis fungoides, electron energies below 5 MeV are advantageous. These are produced by changing the high atomic number scattering foil to a carbon decelerator. The decelerator decreases the mean energy of the electrons without introducing excessive photon contamination, as it is made of a low atomic number material.

The therapeutic range is in this way decreased to a fraction of one cm with the photon background still below 2 per cent (SVENSSON et coll. 1977).

Discussion and comparisons with other accelerators. In the Appendix is shown that the therapeutic range, R_{85}, increases with the accelerator beam energy to a certain energy and then decreases with further increase in energy. The maximum R_{85} is reached already at 21 MeV if a single foil made of copper is used to obtain a uniform beam (± 5 %) for fields up to 30 cm × 30 cm at SSD = 100 cm (Table 3). The maximum useful energy and also the largest R_{85} for a given uniformity increase with the atomic number, Z, of the scatterer, suggesting a high Z-material to be chosen. The experimental values of R_{85} measured on therapy accelerators are even lower than

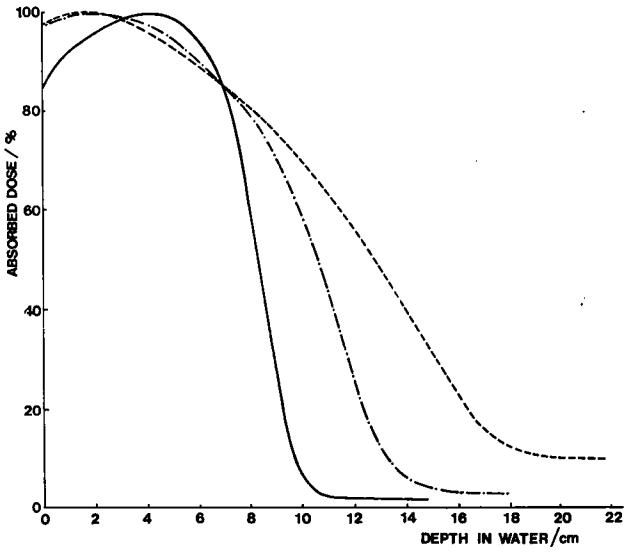

	R_{85}/cm	E_0/MeV	$(E_p)_{0,}$/MeV	$\bar{E}_0$/MeV
Betatron Örebro	7.0	36.2	34.3	29.7
———	7.0	27.5	26.3	24.5
Microtron factory Uppsala	7.0	20.9	19.7	19.5

Fig. 7. Central axis depth dose distributions at $(E_p)_0 = 26.3$ MeV and 34.3 MeV, SSD = 100 cm and ⌀ 15 cm for a betatron. Scattering foils of lead were used. The microtron curve was measured at 19.7 MeV, SSD 100 cm and 22 cm × 22 cm and the dual foil system was used. All of the curves have about the same therapeutic range, R_{85} = 7.0 cm.

those estimated in the appendix. The reasons for this discrepancy are the approximate nature of the mass scattering power formula eq. (22) and the fact that bremsstrahlung generated in the foil has not been taken into full account in the appendix. Furthermore the practical geometry will often include scattered electrons from the collimators in the treatment field as is the case with the betatron measurements in Fig. 7. The maximum R_{85} value for the betatron using a field size with a diameter of 15 cm and lead scattering foils is thus not more than 7 cm. The R_{85} as a function of the energy thus gives a broad maximum for this betatron with almost the same value at 27 and 36 MeV in agreement with the results of the appendix. In Fig. 8 a similar comparison is made but this time with beams of the same practical range showing the loss in therapeutic range for a given most probable electron energy at the surface. It is observed that one of the linear accelerator curves almost coincides with the microtron curve. It can thus be concluded that the energy spread of this travelling wave linear accelerator, using a scanning electron beam to produce uniform dose distribution, is nearly the same as that of a microtron using a dual scattering foil system.

The choice of foil material in the beam of the microtron is not too critical as a dual foil system is used and the total thickness of the foils is low. Uranium and gold are used as the primary scatterers. The secondary foil is made of aluminium as it is fairly thin and must be shaped to give optimum uniformity. Electrons scattered from the collimator will give a negligible contribution to the beam due to the special construction of the collimator. This beam geometry has made it possible to achieve the same therapeutic range with a 20.9 MeV microtron beam energy as with a 27 or 36 MeV betatron beam (Fig. 7). Furthermore, the foil system used in the

	R_p/cm	R_{50}/cm	R_{85}/cm
Betatron Umeå	10.0	8.2	6.2
Linac Gothenburg	10.0	8.2	5.9
Microtron factory Uppsala	10.0	8.6	7.4
Linac Paris	10.0	8.5	7.2

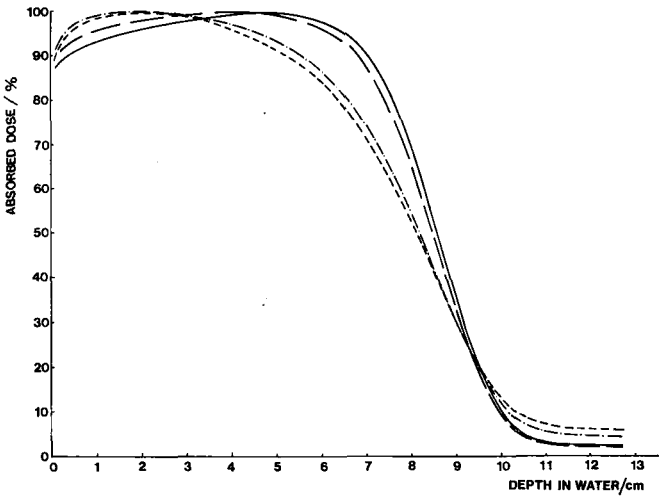

Fig. 8. All of the curves are for large beam sizes and SSD = 100 cm. The practical extrapolated ranges are about the same, i.e. 10.0 cm which means that $(E_p)_0 \approx$ 20.0 MeV. The therapeutic ranges, R_{85}, differ for the three accelerators, being largest for the microtron.

microtron will allow a uniform beam of 40 cm diameter as compared with the 15 cm diameter beam of the betatron.

In Fig. 9 the therapeutic range, R_{85}, appears as a function of the most probable energy at the phantom surface. The values are given for the microtron, a travelling wave linear accelerator and a betatron. The figure shows that the microtron beam gives a linear increase of R_{85} up to the highest available energy 21.9 MeV.

The dose gradients are presented for the same accelerators in Fig. 10. The significance of different dose gradient values is apparent from the depth dose curves in Figs 7 and 8. A considerably larger difference between the microtron and several other accelerators exists at these high energies, compared to the relatively smaller differences found previously at 10 MeV (BRAHME et coll.). A more complete set of data for different types of betatrons and linear accelerators was given previously by BRAHME & SVENSSON (1976 a).

The dose gradient for a monoenergetic wide beam with SSD = 100 cm could be determined from the microtron measurements as the energy degradation of the beam is known as well as the energy spread in the crude accelerator beam, cf. eq. (4). The experimental values differ only slightly from those derived from depth dose curves calculated with the Monte Carlo technique by BERGER & SELTZER (1969) except at the low energies (Fig. 10).

Photon beam

Among the most important properties of the distribution of absorbed dose in a clinical photon beam are: a low surface dose, a considerable build up depth, a narrow penumbra and a high degree of dose uniformity at all depths and field sizes.

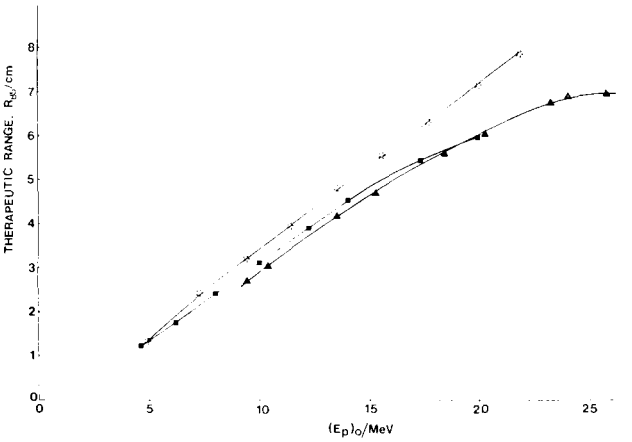

Fig. 9. The variation of the therapeutic range with most probable electron energy at the phantom surface. It is clear, as shown in the appendix, that the betatron which only uses one scattering foil gains very little in therapeutic range by increasing the energy above some 25 MeV. The data are valid for broad beams at SSD 100 cm. Open stars: Microtron, factory Uppsala. Full squares: Linac, Gothenburg. Full triangles: Betatron, Umeå.

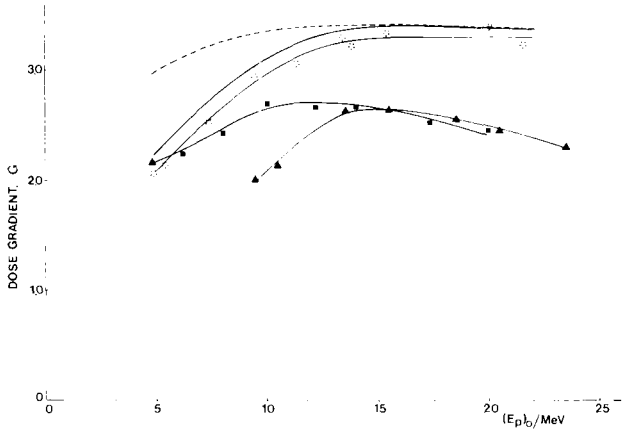

Fig. 10. The variation of the dose gradient with the most probable electron energy at the phantom surface. The theoretical (dashed) curve (Berger & Seltzer 1969) for a monoenergetic beam agrees very well above some 10 MeV with the microtron data adjusted according to eq. (4) for the energy spread in the beam (solid curve). The dose gradient is obviously a sensitive figure of merit of the quality of the electron beam. Symbols as in Fig. 9. Broad beams at SSD 100 cm.

Definitions. A typical central axis depth absorbed dose curve for a 10 MV photon beam is given in Fig. 11. Four different characteristics of a photon depth dose curve in the standard geometry of 10 cm × 10 cm field size and 100 cm SSD are defined in this figure: the surface dose (D_s) as measured at a depth of 0.05 cm of water, the depth of dose maximum R_{100}, the half value depth R_{50} and finally the ratio of the absorbed dose at 10 and 20 cm of depth D_{10}/D_{20}. The ratio taken at 5 and 15 cm, D_5/D_{15}, may equally well be used at beam energies from 10 MV and below as it generally has the same value. The D_{10}/D_{20} ratio has the advantage of being directly related to the practical or effective attenuation coefficient of the photon beam:

$$\mu_p = d \ln \left(\frac{D_{10}}{D_{20}} \right) \tag{14}$$

as the 10 and 20 cm depths are on the exponential section of the depth dose curve for all beam energies below 40 MV ($d = 0.1$ cm^{-1}). One further reason for the use of

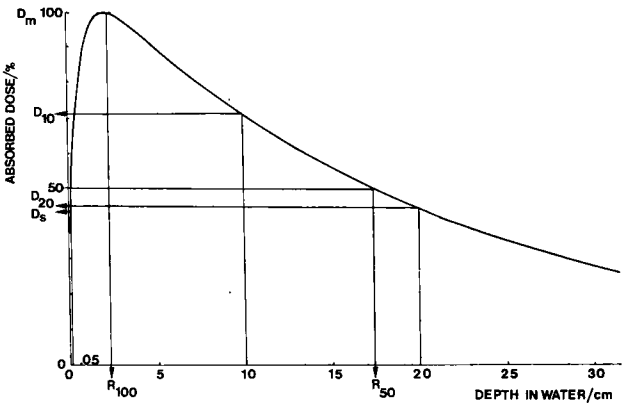

Fig. 11. Central axis depth dose curve for a typical 10 MV photon beam with definitions of all parameters used in the text. D_m is the maximum absorbed dose, D_s the surface dose measured at 0.05 cm depth, R_{100} the depth of dose maximum and R_{50} the half value depth. The dose ratio D_{10}/D_{20} (or D_5/D_{15}) may be used to obtain the practical or effective attenuation coefficient μ_p eq. (15) of the photon beam.

D_{10}/D_{20} ratio above 10 MV is that the reference depth in this energy range is 10 cm, but 5 cm is sometimes used below 10 MV (NACP 1972). The arguments behind the use of the 0.05 cm depth for the specification of the surface dose D_s are the same as have been mentioned previously for electron beams BRAHME & SVENSSON 1976 a. Most important is that the mean depth of the radiation sensitive layers below epidermis are of this order of magnitude (ORTON & SEIBERT 1972), thus making the surface dose an important concept for the estimation of skin-sparing effect. Another important reason is that this depth is accessible with most conventional high accuracy dosimetry systems, whereas the dose at the very surface is difficult to measure due to the interface problems (BERTILSON 1975). The uniformity of the photon beam is defined in the same way as for the electron beam, namely as the ratio of the areas inside the 90 and 50 per cent isodose levels at the reference depth (NACP 1977).

Analytic description of the depth dose curve. A semi-empirical description of the depth dose distribution of a high energy photon beam was introduced by JOHNS et coll. (1949). A slightly more general expression, which normally can be fitted to a measured distribution with an accuracy better than one per cent, is given by

$$D(z) = D_c(e^{-\mu_p z} - \nu e^{-\mu_e z}) \tag{15}$$

where

$$D_c = \frac{D_m}{e^{-\mu_p R_{100}} - \nu e^{-\mu_e R_{100}}} \tag{16}$$

The characteristic attenuation coefficient μ_p is related to the absorption of the primary photons and the similar coefficient μ_e to the absorption of secondary electrons generated by the photons. The value of μ_p is accurately given by eq. (14). Similarly, as a first approximation, μ_e and ν can be estimated from

$$\nu \approx 1.1 - \frac{D_s}{D_m} \tag{17}$$

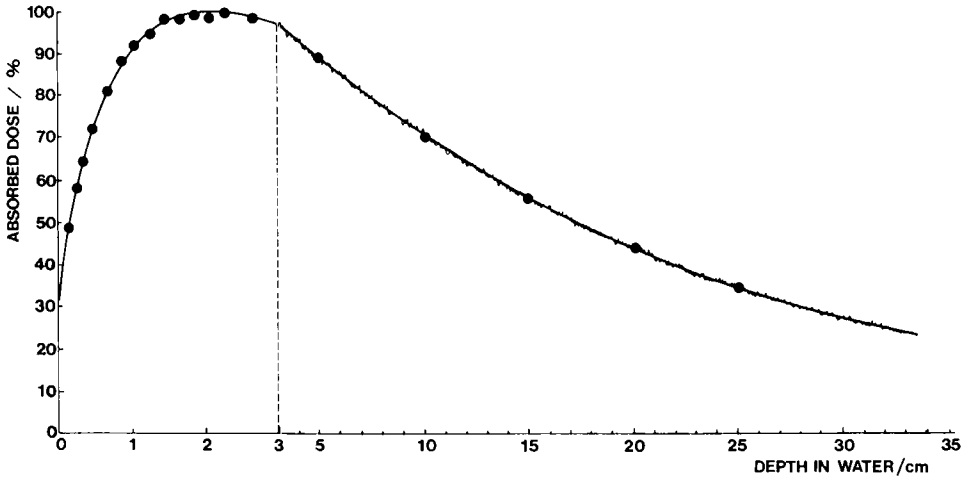

Fig. 12. Central axis depth dose curve at 10.2 MV, SSD = 100 cm and 10 cm × 10 cm. The semiconductor (jagged line) and liquid ionization chamber (●) measurements agree well at depths beyond dose maximum. The curves are displaced relative to each other by somewhat less than 1 mm at smaller depths (not indicated in the figure). If the parameters stated in Table 2 are used in eq. (15) a depth dose curve (solid line) with a very good fit to the experimental data is obtained.

and

$$\mu_e \approx \frac{1}{\nu D_c}\left(\frac{dD}{dz}\right)_0 + \frac{\mu_p}{\nu} \tag{18}$$

When the values of these parameters are found which give the best fit to the experimental data, the depth of dose maximum can be obtained accurately from:

$$R_{100} = \frac{\ln \frac{\mu_e}{\mu_p}\nu}{\mu_e - \mu_p} \tag{19}$$

The effective attenuation coefficient μ_p thus obtained is a very useful parameter when corrections must be made for heterogeneities or for oblique incidence, for example in dose planning. According to elementary considerations it should be expected that the photon dose from a point source should decrease as the product of an inverse square law factor depending on the source to surface distance and an exponential factor containing the mean attenuation coefficient of the photon spectrum. It can be shown that these two factors can be replaced with high accuracy by a single exponential factor containing the practical or effective photon attenuation coefficient μ_p. The mean attenuation coefficient $\bar{\mu}$ of the photon spectrum can be estimated from μ_p by subtracting twice the inverse value of the source to surface distance. Due to its high accuracy over the entire depth interval (cf. Fig. 12), the parameters of eq. (15) are ideal as quality parameters for comparison, check and

Table 2

Photon beam characteristics

Accelerator	E_a MeV	μ_p m^{-1}	D_{10}/D_{20}	D_5/D_{15}	R_{100} cm	R_{50} cm	μ_e cm^{-1}	ν	$\frac{D_s}{D_m}$	ϱ	Reference
Van de Graaff	2	7.87	2.18	2.12	0.4	11.1	0.38	0.17		0.994	HPA (1972)
^{60}Co		6.79	1.97	1.95	0.5	12.1	0.52	0.12		0.981	HPA (1972)
Van de Graaff	4	6.12	1.84	1.82	1.0	13.7	0.50	0.12		0.996	HPA (1972)
Linac	4	6.31	1.88	1.87	1.0	13.3	0.88	0.56		0.985	CASTRO et coll. (1972)
Linac	6	5.33	1.70	1.70	1.8	15.4	1.78	0.70	0.41	0.977	HOLT et coll. (1970)
Linac	6	5.46	1.73	1.73	1.8	15.4	1.80	0.69	0.43	0.962	HPA (1972)
Linac	8	4.93	1.64	1.64	2.2	17.0	1.84	0.76	0.34	0.989	HPA (1972)
Linac	8	5.08	1.66	1.65	2.3	17.0	0.99	0.47	0.66	0.992	CHAN et coll. (1973)
Linac	8	4.99	1.65	1.65	1.8	16.5	1.22	0.33	0.78	0.997	IAEA 1976
Microtron	10	4.72	1.60	1.60	2.1	17.5	1.59	0.72	0.37	0.997	Present work
Linac	10	4.69	1.60	1.60	2.3	17.8	1.47	0.91	0.18	0.989	CONNOR et coll. (1976)
Linac	10	4.63	1.59	1.59	2.4	18.2	1.30	0.76	0.33	0.988	KHAN et coll. (1972)
Linac	10	4.49	1.57	1.56	2.6	18.8	1.29	0.90	0.18	0.999	KELLER et coll. (1975)
Linac	15	4.24	1.53	1.52	2.7	20.1	1.16	0.81	0.27	0.999	HPA (1972)
Linac	16	4.28	1.53	1.53	2.6	19.9	0.92	0.47	0.64	0.993	IAEA (1976)
Linac	18	4.05	1.50	1.49	2.9	20.9	1.02	0.67	0.43	0.998	NOEL et coll. (1976)
Betatron	20	4.09	1.50	1.48	3.3	21.6	0.75	0.59	0.53	0.993	HPA (1972)
Microtron	21	4.29	1.53	1.53	3.0	20.3	1.06	0.80	0.29	0.997	Present work
Betatron	24	3.73	1.45	1.42	3.9	23.8	0.79	0.89	0.17	0.997	HPA (1972)
Linac	25	4.09	1.50	1.47	3.7	22.1	0.75	0.74	0.35	0.988	PODGORSAK et coll. (1974)
Linac	25	3.79	1.46	1.43	3.7	23.3	0.79	0.78	0.30	0.993	TAPLEY (1973)
Betatron	25	3.75	1.45	1.38	4.7	24.9	0.60	0.85	0.22	0.999	PODGORSAK et coll. (1974)
Synchro-tron	30	3.95	1.47	1.38	4.7	24.3	0.49	0.67	0.45	1.000	MITCHELL et coll. (1953)
Betatron	31	3.52	1.42	1.36	4.7	25.9	0.68	1.05	—	0.998	HPA (1972)
Betatron	35	3.33	1.39	1.33	4.9	27.4	0.67	1.13	—	0.995	HPA (1972)
Betatron	35	3.57	1.43	1.40	4.0	24.9	0.74	0.78	0.30	0.995	NACP (1972)
Betatron	42	3.61	1.43	1.36	4.2	25.6	0.49	0.50	0.64	0.999	NACP (1972)
Betatron	45	3.54	1.42	1.35	4.4	26.1	0.50	0.49	0.60	0.999	NACP (1972)

specification of the beam quality and for computerized treatment planning. For such applications the coefficients of eq. (15) can be obtained somewhat more accurately by repeated exponential regression, which has been used in Fig. 12 to find the best fit to the measured data points according to the method of least squares. Data from such an analysis of a number of published depth dose curves are listed in Table 2.

All beams have been evaluated for SSD = 100 cm and a field size of 10 cm × 10 cm.

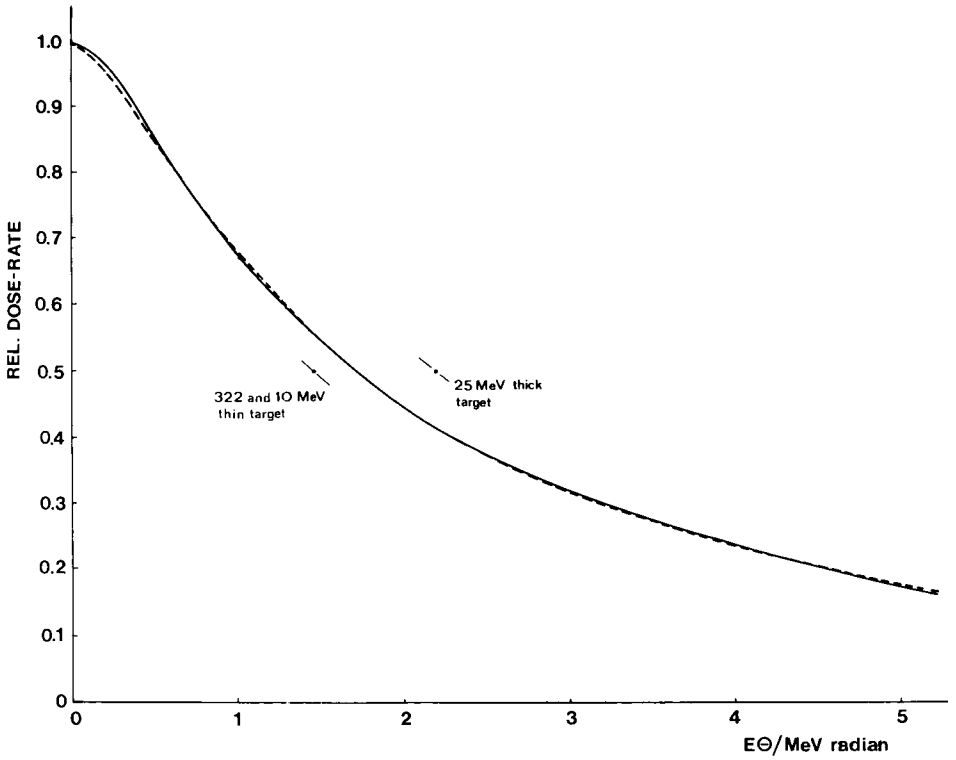

Fig. 13. Dose distribution without flattening filter in a plane perpendicular to the beam axis at 3 cm depth was measured (SSD = 100 cm) and compared with the literature and the curve from eq. (20) (---).

The last column contains the regression coefficient of the fit. It characterizes the goodness of the fit of the build-up section as the regression coefficient of the fall-off is practically at unity in most cases.

Target. The target design is of great importance for the quality of the photon beam. It is generally desirable that the target produce a hard photon spectrum with the widest possible directional distribution of both the high energy and low energy photons so that unnecessarily thick flattening filters can be avoided. These conditions are best fulfilled by a thin high Z target with a thickness selected to obtain simultaneously a high bremsstrahlung conversion efficiency in the forward direction and wide directional distribution of the high energy photons. This optimum is obtained with a target thickness of around one third of the electron range (LANZEL & HANSSON 1951, BERGER & SELTZER 1970). The electrons that penetrate the target are easily stopped in a low Z absorber which produces a minimum of low energy photons and does not stop the high energy photons as much as would a high Z absorber. The photon distribution obtained from such a target will have a

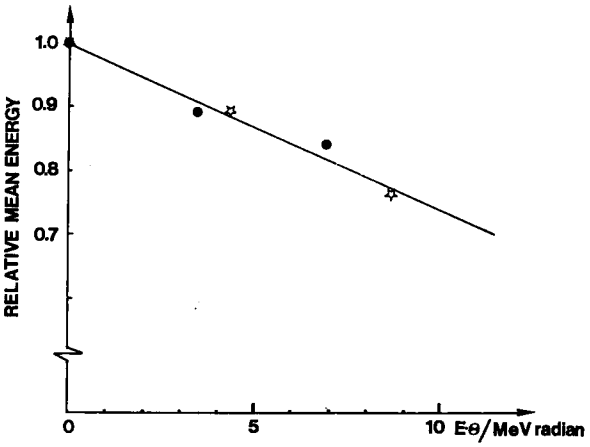

Fig. 14. Variation of the mean photon energy of a 21 MV bremsstrahlung beam with the angle from the axis of the incident electron beam. The angle is expressed in MeV radians as explained in the text to simplify extrapolation to other energies.

directional dependence both with regard to its energy fluence rate and its mean energy.

The variation of the absorbed dose rate (and approximately of the energy fluence rate) with the angle, measured from the direction of the incident electron beam, is plotted in Fig. 13. This lateral dose distribution can be approximated by a simple semi-empirical relation:

$$D(\theta) = \frac{D_m}{1 + \left(\frac{E\theta}{a}\right)^b} \tag{20}$$

where θ is the angle in radians, E the accelerator energy in MeV, 'a' the half value angle in MeV-radians and 'b' a constant.

By using the product of angle and energy the constant a gets a very small energy dependence as both the photon production and the electron multiple scattering processes produce angular deflections which decrease inversely with electron energy. This is also clearly demonstrated by the additional data points for the half value angle, a, of 322 MeV (ROSENGREN 1952) and 10 MeV thin target bremsstrahlung and the 25 MeV thick target bremsstrahlung (PODGORSAK et coll. 1974). The values of a and b which give the best fit to the experimental curve at 21 MeV are a = 1.73 MeV radians and b = 1.4. The maximum deviations obtained are less than one per cent for angles below 5 MeV radians.

In Fig. 14 the mean photon energy is plotted as a function of the product of energy and emission angle. The calculations are based on the Schiff formula (SCHIFF 1951) for thin target bremsstrahlung and are corrected for multiple electron scattering in the target (BRAHME 1975). The experimental points are estimated from dose distributions measured by PODGORSAK et coll. It is clear that for large fields and high accelerator energies the variation of the mean energy across the field is considerable.

Flattening filter. The fact that the mean energy is highest in the forward direction close to the central axis where the energy fluence rate is also peaked is a situation which has generally been overlooked and has instead been aggravated by using thick low Z flattening filters. The result of such a field flattening method is fields of good uniformity at one particular depth but hot spots at smaller depths and rounded corners in the isodose distribution at larger depths. However, such a filter produces the hardest possible photon distribution along the central axis which is useful for production of small fields with deep dose maxima (PODGORSAK et coll.).

If instead the goal is to obtain large uniform photon beams at all depths, the flattening filter should be designed to give the same mean energy in all directions or perhaps a somewhat higher energy at the periphery to compensate for the increased penetration distance. This result may be obtained by selecting a high Z material in the center of the beam and low Z material closer to the periphery to control simultaneously the spectrum and the intensity of the photons (BRAHME & SVENSSON 1976 c). Such a filter has the further advantage that it makes efficient use of the available space since a high density and high Z material are used in the central region where the greatest filtration is needed. In this way flattening filters of an almost constant thickness can be made.

Dose distributions

Dosimetry. Depth dose curves in a water phantom measured with diode and liquid ionization chamber were compared at 10 MV (Fig. 12). The measurements agreed at depths beyond about 1 cm but differed somewhat at small depths. The difference corresponds to a displacement of the curves of about 1 mm and may partly be the result of an uncertainty in the determination of the effective measurement points for the two dosimeters. The two dosimeters have also been compared with $FeSO_4$ measurements at and beyond dose maximum for ^{60}Co, 21 MV and 32 MV. The agreement is better than 2 per cent. The isodose and depth dose curves were measured with a diode and should therefore have an uncertainty of less than 2 per cent at depths greater than dose-maximum, and the uncertainty in the geometrical position of the dose levels in the build-up region should be less than 1 mm.

Off-axis flattening. The target and flattening system described gives a high degree of dose uniformity at all depths, i.e., the isodoses do not have hot spots at small depths or rounded corners at large depths even if very large fields are used (Fig. 15). The uniformity index varies from 0.97 to 1.03 for field sizes between 10 cm × 10 cm and 40 cm × 32 cm if the definition used by the NACP (1972) is used. These values are higher than for any of the 14 accelerators investigated by SVENSSON & HETTINGER (1971) and exceed by a large margin the recommendations given by the NACP, i.e. 0.80. If the proposed new definition of the uniformity index (NACP 1977) is used, the values become 0.87 to 0.98 for the field size range given.

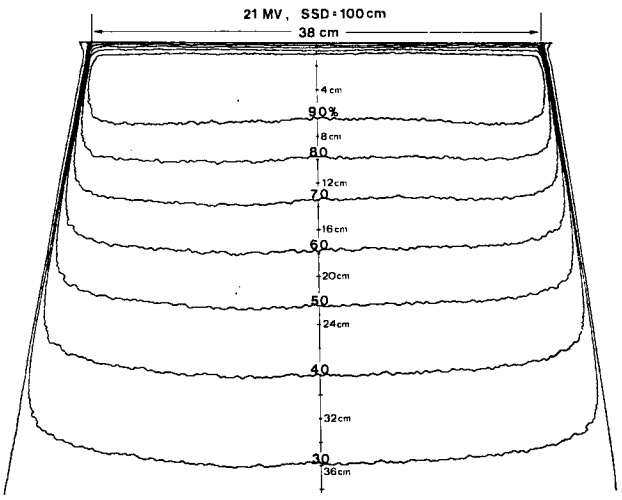

Fig. 15. The target flattening filter system used makes it possible to produce large uniform beams up to 42 cm × 37 cm, at SSD = 100 cm. The uniformity is good at all depths and field sizes.

Depth dose curves. In Table 2 characteristics of photon depth dose curves are given for a few different accelerators according to the parameter definitions of Fig. 11. The surface dose, D_s/D_m is determined from the experimental values, making use of eq. (15) for the extrapolation down to 0.05 cm. The large values of the regression coefficients indicate that this extrapolation method is fairly accurate at least for energies above 4 MV. The D_s/D_m ratio decreases for most accelerators when the energy is increased, but there are a few exceptions. The differences between various types of accelerators are much larger than could be explained from pure dosimetric uncertainties but could probably be explained by the differences in locations and dimensions of flattening filters and collimators. Relatively low values are obtained for the microtron beams at 10 and 21 MV.

Several measures of the penetrative power of photon beams have been suggested. Thus, the IEC (1977) will probably use the half value depth, R_{50}, the NACP (1972) recommended D_5/D_{15} and D_{10}/D_{20} is in the present report suggested for use at least above 10 MV. It has been shown previously that a harder spectrum is obtained along the central ray if low atomic number target and flattening filter are used (PODGORSAK et coll. 1974). However, this target-filter combination means a softer spectrum at larger angles with the central axis of the beam and makes it impossible to create a beam of high uniformity at all depths. In our opinion a very good uniformity is to be preferred to a small increase in the R_{50} or R_{100}. Thus the R_{50} would only increase from 20.3 cm to about 22.0 cm if a target-flattening filter combination of aluminium were used instead of the system described.

Discussion and Conclusions

The 22 MeV microtron used for the measurements has now (May 1977) been tested in the factory for almost a year. Not all of the accessories for the irradiations

are as yet ready, but they are in their latest stage of manufacture. However, it could be concluded that the accelerator has until now functioned very well. It has also been shown that the special qualities of this accelerator should make it an attractive choice as a medical accelerator.

The physical size of the microtron will be large for electron energies over some 20 MeV. The largest convenient size is therefore probably reached with this type of microtron as the diameter of the disk shaped accelerator is about 2 m. However, its special shape makes it possible to locate the accelerator in relatively small rooms (SVENSSON et coll. 1977). Other types of microtrons which accelerate electrons by one or several MeV per revolution may be build for radiation treatments in the high energy region. Among these are the conventional microtrons with 'Russian' injection (KAPITZA et coll. 1962) or with shorter microwave length (KAISER & MEYES 1955) and the race-track microtrons (MACDONALD & FROELICH 1974), which seem ideal as electron sources for radiation therapy at the highest energies.

It may be claimed that there is not a great need of accelerators which give energies over about 20 MeV. For example 85 per cent of the electron treatments at the university hospitals of Umeå and Stockholm are given with electron energies below 20 MeV even though energies up to 40 MeV are available, and about the same percentages are valid for other hospitals in Sweden. Furthermore, as the therapeutic range of the 22 MeV microtron electrons is greater than that for the 35 MeV and 42 MeV betatrons used here today, it could be concluded that almost all treatments given today could be carried out with the 22 MeV microtron. However, as the shape of the microtron depth dose curves at high energies is different from those of many betatrons and linear accelerators, the distributions for energies higher than 22 MeV may also turn out to be of great interest.

The specifications for the 22 MeV microtron were first laid out by the hospital in Umeå. It may turn out that other specifications are required by other hospitals. An example of varying opinions at different hospitals may be found in the choice between a very penetrative roentgen ray beam at the centre of the beam and a very uniform beam at all phantom depths but a slightly softer spectrum in the central part of the beam. However, changes in the target-flattening filter system are fairly simple to carry out and can therefore be adjusted to the special needs of the hospital.

Appendix

Maximum useful accelerator energy

For high electron energies the problem of obtaining beams of high quality becomes increasingly difficult. This is so mainly because the amount of scattering material needed to produce a beam of high uniformity increases rapidly with electron energy due to the rapid decrease of the mass scattering power with energy.

The relatively thick scatterers needed at high energies will naturally degrade the electron beam so that a compromise generally has to be found between a good dose uniformity

Table 3

Maximum useful accelerator energy using only one scattering foil (cf. Appendix)

Foil material	$S_{col}X_0$ (MeV)	E_0 (MeV)	R_{85} (cm)
Cu	20.6	21	4.1
W	9.13	45	8 7
Pb	8.66	47	9.2
U	7.80	54	10.3

across the beam and a large therapeutic range and consequent good dose uniformity along the beam.

The scattering foil thickness and the concomitant energy loss and energy straggling increase approximately with the square of the beam energy when only a single scattering foil is used. For this reason it is not of interest to increase the accelerator energy over a certain limit as a further increase no longer results in an increase in therapeutic range. This limit may be calculated from eq. (13) and a relation giving the necessary foil thickness and most probable energy loss for a given degree of uniformity. Assuming a purely gaussian angular distribution of the scattered electrons, the necessary mean square angle of scattering, $\overline{\theta^2}$, for a uniformity of $\pm 5\%$ over a maximum angular interval of $\pm\theta_m$ is obtained from:

$$\exp\left(-\left(\frac{\theta_m^2}{\overline{\theta^2}}\right)\right) = 0.9 \tag{21}$$

The necessary foil thickness, t, can now be estimated using the simple relation for the scattering power given by Rossi:

$$\frac{\overline{\theta^2}}{t} = \frac{E_s^2}{E_0^2 X_0} \tag{22}$$

The resulting most probable energy loss thus becomes:

$$E_0 - E_p = S_{col} X_0 \frac{E_0^2}{E_s^2}\overline{\theta^2} \tag{23}$$

After introducing this expression into eq. (13) the therapeutic range may be written:

$$R_{85}(E_p, \Gamma) = \left(1 - \frac{0.85}{G_0}\right) kE_0 - \left(k_2 + \frac{k_1}{c_f}\right) S_{col} X_0 \frac{E_0^2 \overline{\theta^2}}{E_s^2} \tag{24}$$

where c_f is the constant of proportionality between energy loss and energy spread in the scattering foil.

This expression has maximum for:

$$E_0 = \frac{\left(1 - \frac{0.85}{G_0}\right) E_s^2 k}{2S_{col} X_0 \overline{\theta^2}\left(k_3 + \frac{k_1}{c_f}\right)} \approx \frac{k_4}{S_{col} X_0 \overline{\theta^2}} \tag{25}$$

where $k_4 = 170$ (MeV)^2 assuming the following values of the constants: $G_0 = 3.4$, $E_s = 21.2$ MeV and $c_f = 2.5$ ($c_f = 3$ for Cu).

The maximum therapeutic range thus becomes

$$R_{85} = \left(1 - \frac{0.85}{G_0}\right)^2 \frac{k^2 E_s^2}{\left(k_3 + \frac{k_1}{c_f}\right) 4 S_{col} X_0 \bar{\theta}^2} \approx \frac{k_5}{S_{col} X_0 \bar{\theta}^2} \tag{26}$$

where $k = 33$ MeV cm.

The largest therapeutic range is therefore obtained for the material with smallest possible collisional energy loss per radiation length, i.e. for high atomic number materials.

Typical values for these parameters are given in Table 3 for a uniformity of $\pm 5\%$ over a square field of 30 cm by 30 cm or which give the same values $\pm 2.5\%$ over a 20 cm by 20 cm field. However, it should be pointed out that these results are only approximate as the photon contamination has not been included in the analysis. If the effect of the photons were taken into account the results would be even worse as both the therapeutic range and the uniformity is decreased by the presence of the photons.

SUMMARY

The properties of the electron and photon beams from a 22 MeV clinical microtron are presented. Favourable isodose distributions for radiation therapy are obtained for both modalities. For the electron beam this is accomplished using a dual scattering foil system in which the secondary foil is shaped to optimize uniformity and minimize energy loss and energy straggling. The photon beam is flattened by a composite filter to produce dose distributions of high uniformity over a wide depth interval.

ZUSAMMENFASSUNG

Die Eigenschaften der Elektron- und Photonstrahlen für ein 22 MeV klinisches Mikrotron werden gegeben. Vorteilhafte Isodosis-Verteilungen für die Strahlentherapie werden für beiden Modalitäten erhalten. Für den Elektronenstrahl wird das durch Verwendung eines zweifachen Streu-Foliensystem erreicht, bei welchem die sekundäre Folie geformt ist um eine Gleichförmigkeit zu optimieren und den Energieverlust und die Energie zerstreuung auf ein Minimum zu bringen. Der Photonstrahl ist durch einem zusammengesetzten Filter abgeflacht, um Dosisverteilungen von hoher Gleichförmigkeit über ein grosses Tiefen-Interval zu erhalten.

RÉSUMÉ

Les auteurs présentent les propriétés des faisceaux d'électrons et de photons d'un microtron clinique de 22 MeV. On obtient des distributions isodoses favorables pour le traitement par les radiations pour ces deux modalités. Pour le faisceau d'électrons, ceci est obtenu par un système de deux écrans diffusants dans lequel l'écran secondaire est formé pour optimiser l'uniformité et minimiser la perte d'energie et le 'straggling' d'énergie. Le faisceau de photons est égalisé par un filtre composite pour donner des distributions de doses d'une grande uniformité sur un large intervalle de profondeur.

REFERENCES

ATHERTON L.: Depth absorbed dose distributions for electrons. Phys. in Med. Biol. 21 (1976), 453.

— und CALAMINI A.: Einfluss konstruktiver Merkmale auf die medizinisch-physikalischen Parameter bei einem linearen Elektronenbeschleuniger. Deutscher Roentgenkongress, Essen 1976. AED Conf. 168–004.

BARONCELLI G.: I microtroni. (In Italian.) Rad. alta Energia 13 (1974), 119.

BERGER M. J.: Monte Carlo code system for electron and photon transport through extended media. RSIC-CCC-107, p. 57. Oak Ridge National Laboratory 1969.

— and SELTZER S. M.: Quality of radiation in a water medium irradiated with high-energy electrons. Book of abstracts, p. 127. Twelfth International Congress on Radiology, Tokyo 1969.

— — Bremsstrahlung an photoneutrons from thick tungsten and tantalum targets. Phys. Rev. C2 (1970), 621.

BERTILSON G.: Electron scattering effects on absorbed dose measurements with LiF-dosimeters. Thesis, Institute of Radiation Physics, Lund, Sweden 1975.

BJÄRNGAARD B. E., PIONTEK R. W. and SVENSSON G. K.: Electron scattering and collimation system for a 12 MeV linear accelerator. Med. Phys. 3 (1976), 153.

BLUNCK O. und WESTPHAL K.: Energieverlust energiereicher Elektronen in dünnen Schichten. Z. Physik 130 (1951), 641.

BRAHME A.: Multiple scattering of relativistic electrons in air. TRITA-EPP-71-22. Royal Institute of Technology, Stockholm 1971.

— On the optimal choice of scattering foils for electron therapy. TRITA-EPP-72-17. Royal Institute of Technology, Stockholm 1971.

— Simple expressions for the penetration of high energy electron beams in matter. Report SSI: 1975-011. National Institute of Radiation Protection, Stockholm.

— Electron transport phenomena and absorbed dose distributions in therapeutic electron beams. Livro de resumos, Abstract No. S 0348, p. 198. Fourteenth International Congress on Radiology, Rio de Janeiro 1977.

— and SVENSSON H. (a): Specification of electron beam quality from the central axis depth absorbed dose distribution. Med. Phys. 3 (1976), 95.

— — (b): Depth absorbed dose distributions for electrons. Phys. in Med. Biol. 21 (1976), 304.

— — (c): Methods of improving dose uniformity in high energy photon and electron beams. Digest Fourth ICMP. Phys. Canada 32 (1976), 28.3.

— HULTÉN G. and SVENSSON H.: Electron depth absorbed dose distributions for a 10 MeV clinical microtron. Phys. in Med. Biol. 20 (1975), 39.

BREUER H.: Energieverlust von Elektronen in Aluminium im Energiebereich 20 bis 60 MeV. Z. Physik 180 (1964), 209.

BRIOT E. et DUTREIX A.: Dosimétrie des faisceaux d'électron de haute énergie d'un accélérateur linéaire. J. Radiol. Électrol. 57 (1976), 447.

CASTRO V. G. and KOPENHAVER J. F.: Some aspects of dosimetry with a 4 MV linear accelerator. Radiology 102 (1972), 691.

CHAN F. K., HAYMOND H. R., KAGAN A. R., CARBONE G. E. and GEORGE F. W.: Comparative beam data for the 25 MV betatron, 8, 6, and 4 MV linear accelerators and Co-60 units. Radiology 109 (1973), 691.

CONNOR W. G., HICKS J. A., BOONE M. L. M., MAYER E. G. and MILLER R. C.: 10 MV X-ray beam characteristics from a new 18 MeV linear accelerator. Int. J. radiat. Oncol. Biol. Phys. 1 (1976), 705.

DIN 6809. Klinische Dosimetrie. Blatt 1 (1975), 9.

DOLPHIN G. W., GALE N. H. and BRADSHAW A. L.: Investigation of high energy electron beams for use in therapy. Brit. J. Radiol. 32 (1959), 13.

HARDER D.: Spectra of primary and secondary electrons in material irradiated by fast electrons. IAES Techn. Rep. Ser. No. 58 (1966), 140.

HERRING D. F. and COMPTON D. M. J.: The degree of precision required in the radiation dose delivered in cancer radiotherapy. *In:* Computers in radiotherapy, p. 51. British Institute of Radiology, London 1971.

HOLT J. G., LAUGHLIN J. S. and MORONEY J. P.: The extension of the concept of tissue-air ratios (TAR) to high-energy X-ray beams. Radiology 96 (1970), 437.

HPA (Hospital Physicists' Association): Central axis depth dose data for use in radiotherapy. Brit. J. Radiol. (1972), Suppl. No. 11.

HULTÉN G.: A comparison between absorbed dose distributions measured with Scanditronix radiation field analyzer RFA-1 and conventional methods. Proceedings of NACP meeting, Reykjavik, Iceland 1975.

IAEA Radiation Dosimetry Data Catalogue, 2.7.2 (1976).

ICRU (International Commission on Radiation Units and Measurements) Report 21 (1972).

— Report 24 (1977).

IEC (International Electrotechnical Commission) 62 C (Secretariat) 10 (1977).

JOHNS H. E., DARBY E. K., HASLAM R. N. H., KATZ L. and HARRINGTON E. L.: Depth dose data and isodose distributions for radiation from a 22 MeV betatron. Amer. J. Roentgenol. 62 (1949), 257.

KAISER H. E. and MAYES W. T.: General purpose x-band laboratory microtron with facilities for electron extraction. Rev. sci. Instr. 26 (1955), 565.

KAPITZA S. P., BYKOV V. P. and MELEKHIN V. N.: An efficient high-current microtron. Sov. Phys. JETP 14 (1962), 266.

KARZMARK C. J., LOEVINGER R., STEELE R. E. and WEISSBLUTH M.: Radiation therapy with high energy electrons. Radiology 74 (1960), 633.

KELLER B., BASSANO D., MATHEWSON C. and RUBIN P.: 10 MV photon beam characteristics. Int. J. radiot. Oncol. Biol. Phys. 1 (1975), 69.

KHAN F. M., MOORE V. C. and SATO S.: Depth dose and scatter analysis of 10 MV X-rays. Radiology 102 (1972), 165.

KOZLOV A. P. and SHISHOV V. A.: Forming of electron beams from a betatron by foil scatterers. Acta radiol. Ther. Phys. Biol. 15 (1976), 493.

LANDAU L.: On the energy loss of fast particles by ionization. J. Phys. USSR 8 (1944), 221.

LANZL L. H.: Magnetic and threshold techniques for energy calibration of high energy radiations. Ann. N.Y. Acad. Sci. 161 (1969), 101.

— and HANSSON A. O.: Z dependence of angular distribution of bremsstrahlung from 17 MeV electrons. Phys. Rev. 83 (1951), 959.

MACDONALD J. C. F. and FROELICH H. R.: The race-track microntron. Its potential in radiation therapy. Proceedings of Third Conference on Application of Small Accelerators II, p, 334. Denton, Texas, 1974.

MARKUS B.: Beiträge zur Entwicklung der Dosimetrie schneller elektronen. Strahlentherapie 124 (1964), 33.

MITCHELL J. S., SMITH C. L., ALLEN-WILLIAMS D. J. and BRAAMS R.: Experience with the 30 MeV synchotron as a radiotherapeutic instrument. Acta radiol. 40 (1953), 463.

NACP (Nordic Association of Clinical Physics): Procedures in radiation therapy dosimetry with 5 to 50 MeV electrons and roentgen and gamma rays with maximum photon energies between 1 MeV and 50 MeV. Acta radiol. Ther. Phys. Biol. 11 (1972), 607.

NACP. Private communication. Working group of NACP on electron and photon dosimetry (1977).

NOEL A., DROUARD J., LAUGIER A. et URBAJTEL M.: Étude dosimétrique de l'accélérateur linéaire therac 20 saturne. Proceedings of Fifteenth Meeting of French Hospital Physicists Society, p. 141. Caen, 1976.

ORTON C. G. and SEIBERT J. B.: Depth dose in skin for obliquely incident Co-60 radiation. Brit. J. Radiol. 45 (1972), 271.

PETTERSSON C. and HETTINGER G.: Dosimetry of high energy electron radiation based on the ferrous sulfate dosimeter. Acta radiol. Ther. Phys. Biol. 6 (1967), 160.

PODGORSAK E. B., RAWLINGSON J. A., GLAVINOVIC M. I. and JOHNS H. E.: Design of X-ray targets for high energy linear accelerators in radiotherapy. Amer. J. Roentgenol. 121 (1974), 873.

ROSENGREN J. W.: Angular distribution of bremsstrahlung radiation. U.S. A.E.C., UCRL-1999 (1952).

ROSSI B. B.: High energy particles, p. 52. Prentice Hall, New York 1956.

SCHIFF L. I.: Angular distribution of thin target bremsstrahlung. Phys. Rev. 83 (1951), 252.

SCHRIBER S. O., FUNK L. J. and MOWCHENKO Z. T.: A Monte Carlo calculation of electron depth-dose distribution. Digest Fourth ICMP, Phys. in Canada 32 (1976, 23.2.

SVENSSON H.: Influence of scattering foils, transmission monitors and collimating system on the absorbed dose distribution from 10 to 35 MeV radiation. Acta radiol. Ther. Phys. Biol. 10 (1971), 443.

— and BRAHME A.: Electron beam parameters. Proceedings of AAPM Summer School, Burlington. Massachussetts 1976.

— and HETTINGER G.: Dosimetric measurements at the Nodic medical accelerators., Part I. Characteristics of the radiation beam. Acta radiol. Ther. Phys. Biol. 10 (1971), 369.

— WESTLING P. and LARSSON L.-G.: Radiation-induced lesions of the branchial plexus correlated to the dose-time fraction schedule. Acta radiol. Ther. Phys. Biol. 14 (1975), 229.

— JOHNSSON L., LARSSON L.-G., BRAHME A., LINDBERG B. and REISTAD D.: A 22 MeV microtron for radiation therapy. Acta radiol. Ther. Phys. Biol. 16 (1977), 145.

TAPLEY N.: Characteristics of megavoltage external beams, p. 23. Edited by S. H. Levitt. University of Minnesota Press, Minneapolis 1973.

WERNHOLM O.: The 1200 MeV synchrotron at the University of Lund. Arkiv Fys. 26 (1964), 257.

WICKMAN G.: Radiation quality independent liquid ionization chamber for dosimetry of electron radiation from medical accelerators. Acta radiol. Ther. Phys. Biol. 13 (1974), 37.